Optical properties of HgSe

S. Einfeldt, F. Goschenhofer, C.R. Becker, and G. Landwehr
Physikalisches Institut der Universität Würzburg, Am Hubland, 97074 Würzburg, Germany
(Received 22 July 1994; revised manuscript received 6 October 1994)

The optical properties of HgSe grown by molecular-beam epitaxy have been studied over a wide range of frequencies covering the E_0, E_1, and $E_1+\Delta_1$ gaps. Theoretical calculations of the dielectric function are used in deriving fundamental material parameters for HgSe. The refractive index has thus been determined at room temperature up to 1 eV. A comparison of temperature-dependent measurements of the fundamental absorption in HgSe with theoretical calculations using various sets of band structure parameters has yielded an estimate of the temperature shift of the E_0 gap. The carrier concentration as derived from van der Pauw measurements was shown to be inconsistent with optical determinations of the Fermi energy. Differences in the absolute values of the absorption coefficient compared to theoretical spectra have been observed and compared to data reported for bulk HgSe. The critical point energies E_1 and $E_1+\Delta_1$ could be determined in the temperature range 5–300 K by fitting reflection measurements to theoretical spectra derived from the dielectric function.

I. INTRODUCTION

Recently HgSe was grown successfully by molecular-beam epitaxy (MBE).[1–3] The original motivation for these studies was to make Ohmic contacts to p-type ZnSe with the help of HgSe.[4,5] Besides this technological aspect, HgSe is of special interest for fundamental studies because of its inverted band structure. But apart from some electrical transport measurements, the properties of epitaxial HgSe layers have not previously been studied in detail. In this work we have extensively investigated the optical properties of MBE grown HgSe. The corresponding frequency range covers the fundamental absorption region (E_0 gap) as well as higher critical points in the band structure (E_1 and $E_1+\Delta_1$ gaps). The results are compared with data for bulk HgSe samples reported in the literature. In order to interpret the measurements, theoretical calculations have been carried out. This enables us to find out to what extent the reported band structure parameters are valid in describing our experimental results and to determine fundamental material parameters for epitaxial HgSe, e.g., ϵ_∞, dE_0/dT, $E_1(T)$, and Δ_1.

II. EXPERIMENTAL DETAILS

The epitaxial HgSe layers under consideration were grown on (001) CdTe, ZnTe, or GaAs substrates. Details are described in Refs. 2 and 3. The layer thickness varied from 0.2 to 4 μm and the free electron concentration at helium temperature as determined from van der Pauw measurements was in the range of 1×10^{17}–4×10^{18} cm^{-3}. Transmission and reflection were measured in a Fourier transform spectrometer IFS 88 from Bruker. Unpolarized light was employed and the angle of incidence for the reflection measurements was about 9–10° from the perpendicular.

III. CONTRIBUTION NEAR THE E_0 GAP

A. Theory

The complex dielectric function $\epsilon(\omega)$ near the E_0 gap can be written as a sum of an interband contribution $\epsilon_{\text{inter}}(\omega)$ near the Γ point of the Brillouin zone, an intraband contribution $\epsilon_{\text{intra}}(\omega)$, a contribution from phonons $\epsilon_{\text{phonon}}(\omega)$, and ϵ_∞ which contains the contribution of all higher band transitions (E_0',E_1,E_2,...).

$$\epsilon(\omega)=\epsilon_\infty+\epsilon_{\text{inter}}(\omega)+\epsilon_{\text{intra}}(\omega)+\epsilon_{\text{phonon}}(\omega)\ . \tag{1}$$

In the frequency range under consideration, ϵ_∞ is assumed to be real and constant whereas the phonon contribution is neglected. Within the framework of the random phase approximation, the interband contribution can be written as (see, e.g., Ref. 6)

$$\epsilon_{\text{inter}}(\omega)=\frac{1}{4\pi\epsilon_0}\frac{2\pi e^2\hbar}{m_0^2\omega}\sum_{l\neq m}^{l>m}\frac{1}{(2\pi)^3}\int_{\text{BZ}}d^3\boldsymbol{k}\frac{f(E_l(\boldsymbol{k}))-f(E_m(\boldsymbol{k}))}{\Delta E_{lm}(\mathbf{k})}\left\{\frac{1}{\hbar\omega+\Delta E_{lm}(\boldsymbol{k})+i\Gamma}+\frac{1}{\hbar\omega-\Delta E_{lm}(\boldsymbol{k})+i\Gamma}\right\}$$
$$\times|\langle\psi_l(\boldsymbol{k})|\boldsymbol{\pi}\cdot\boldsymbol{p}|\psi_m(\boldsymbol{k})\rangle|^2\ , \tag{2}$$

where $\Delta E_{lm}(\boldsymbol{k}) = E_l(\boldsymbol{k}) - E_m(\boldsymbol{k})$, $E_l(\boldsymbol{k})$ and $E_m(\boldsymbol{k})$ are the energies of the l and m bands at the wave vector $\boldsymbol{k}$, f is the Fermi-Dirac distribution, $\langle \psi_l(\boldsymbol{k}) | \boldsymbol{\pi} \cdot \boldsymbol{p} | \psi_m(\boldsymbol{k}) \rangle$ is the momentum matrix element for the optical transition between the l and m energy bands, and Γ is the phenomenological broadening parameter of the bands. The integral is to be carried out over the first Brillouin zone (BZ).

The intraband contribution for the approximation of isotropic bands in Ref. 7 is given by

$$\epsilon_{\text{intra}}(\omega) = \frac{e^2}{6\epsilon_0 \hbar^2 \pi^2} \frac{1}{\omega(\omega + i/\tau)} \times \sum_l \int_{\text{BZ}} dk\, k^2 \frac{\partial E_l(k)}{\partial k} \frac{\partial f(E_l(k))}{\partial k} , \quad (3)$$

where τ is the average relaxation time of free charge carriers and the summation is again over all energy bands. Only contributions near the Fermi energy, which always lie in the Γ_8 conduction band for HgSe, contribute to the integral in Eq. (3).

The Fermi energy is calculated by fulfilling the neutrality condition for the charge carriers

$$n - p = N_D - N_A , \quad (4)$$

where n and p are the concentrations of free electrons and holes, respectively, and N_D and N_A are the concentrations of singly ionized donors and acceptors, respectively. The free electron and hole concentrations are given by

$$n = \sum_{\text{CB}} \frac{1}{(2\pi)^3} \int_{\text{BZ}} f(E_{\text{CB}}(\boldsymbol{k})) d^3\boldsymbol{k}, \quad (5)$$

$$p = \sum_{\text{VB}} \frac{1}{(2\pi)^3} \int_{\text{BZ}} [1 - f(E_{\text{VB}}(\boldsymbol{k}))]\, d^3\boldsymbol{k} , \quad (6)$$

where CB and VB stand for the summation over all conduction and valence bands, respectively.

For the description of the band structure we use the Kane model.[8,9] In this model, $\boldsymbol{k} \cdot \boldsymbol{p}$ and spin-orbit interactions for three bands (Γ_6, Γ_7, and Γ_8) are described exactly by neglecting any influence of higher bands ("three band approximation"). Subsequently the $\boldsymbol{k} \cdot \boldsymbol{p}$ interactions with all higher bands are treated by first-order perturbation theory. The anisotropic warping term in the energy bands is taken into account by setting $k_z = 0$ and averaging over k_x and k_y in agreement with the (001) orientation of the samples ("axial approximation"). For the momentum matrix element we have used the expressions given in Ref. 8 which neglect all higher bands. We chose the band model described above because it is the most widely used model in the HgSe literature. Unfortunately previous publications on the HgSe band structure are to some extent contradictory in relation to the large differences in the values of the band parameters. Therefore we have summarized the most important results of the literature in Tables I and II.

Sufficiently high doping levels in HgSe samples require a renormalization of the band structure due to the Coulomb interaction. This effect has been neglected in the HgSe literature and only the Kane band model has been used to describe the properties of all samples independent of their doping levels. We have also followed this procedure and used the Kane model without any corrections. This can be justified by the fact that although the carrier interaction is not explicitly considered it is implicitly contained in the published Kane band parameters listed in Table I. Furthermore, the results of the renormalization should be small compared to the principal inaccuracy of the HgSe band parameters in Table I.

A computation of the integral in Eq. (2) for a given frequency ω results in a significant contribution to the real part of $\epsilon_{\text{inter}}(\omega)$ in the Brillouin zone far removed from the Γ point, e.g., at $E_{\text{CB}}(\boldsymbol{k}) - E_{\text{VB}}(\boldsymbol{k}) \gg \hbar\omega$. However, this band structure model is only an approximation for small values of $|\boldsymbol{k}|$ and the integration interval has to be restricted accordingly. The resulting error in the real part of $\epsilon_{\text{inter}}(\omega)$ is estimated to be about 10%. It is worth mentioning that this problem also occurs in the calculation of the real part of $\epsilon_{\text{inter}}(\omega)$ from the imaginary part by means of the Kramers-Kronig transformation.

Once $\epsilon(\omega)$ has been calculated, the refractive index $n(\omega)$, the extinction coefficient $\kappa(\omega)$, and the absorption coefficient $\alpha(\omega)$ can be determined by means of

$$n(\omega) + i\kappa(\omega) = n(\omega) + i\frac{c}{2\omega}\alpha(\omega) = \sqrt{\epsilon(\omega)} , \quad (7)$$

where c is the velocity of light.

For a given set of band parameters, optical spectra have been calculated for various temperatures as shown in Fig. 1. At lower temperatures two significant absorption edges are to be seen which correspond to the $\Gamma_8^{\text{VB}} \rightarrow \Gamma_8^{\text{CB}}$ and $\Gamma_6^{\text{VB}} \rightarrow \Gamma_8^{\text{CB}}$ (E_0 gap) interband transitions, respectively. The transition $\Gamma_7^{\text{VB}} \rightarrow \Gamma_8^{\text{CB}}$ occurs at about 0.8 eV but cannot be observed in the absorption spectra because of its corresponding small momentum matrix element. The strong increase of the absorption at low photon energies is due to intraband absorption of free charge carriers. The refractive index shows the expected anomalous dispersion ($dn/d\omega < 0$) in the region of band to band transitions. The abrupt decrease and subsequent increase in the refractive index for decreasing photon energies is once again a consequence of the free charge carriers. It should be mentioned that the spectra in Fig. 1 were calculated by assuming the value for ϵ_∞ to be independent of temperature.

The calculated absolute values for the absorption coefficient and the refractive index differ considerably for the various sets of band structure parameters listed in Table I; the resulting absorption coefficient differs by up to a factor of 2 and the refractive index up to 10%. The reason for this is the very large variation in the reported Luttinger parameters which influence the density of states of both the conduction and valence bands.

B. Experimental results

The refractive index for HgSe was determined at 300 K as described in Appendix B for a large number of samples with carrier concentrations in the range $2 \times 10^{17} - 1 \times$

TABLE I. Band structure parameters for HgSe. P is a parameter which is proportional to the matrix component of the momentum between conduction and valence band at $k = 0$, Δ is the energy difference between Γ_8^{VB} and Γ_7^{VB} at $k = 0$ due to spin-orbit interaction, γ_1, γ_2, γ_3, κ, and F are the Luttinger parameters, m_{hh} is the heavy hole mass when determined independently from the Luttinger parameters, and E_{g1} is the $\Gamma_8^{VB} - \Gamma_8^{CB}$ band overlap. The experimental method is listed in the second column: R is reflection, T is transmission, FIR is far infrared, MIR is middle infrared, F/MIR is far and middle infrared, SdH = Shubnikov–de Haas effect, Far is Faraday effect, Hall is Hall effect, Theo is theory, ThM is thermomagnetic effect, MA is magnetoabsorption. RT stands for room temperature. In some of these investigations only a limited number of parameters were determined by means of a fit procedure. In this case the remaining parameters which were taken from the literature were held constant. This is indicated by a referral to the investigation in the corresponding column.

Ref.	Expt.	T (K)	E_0 (eV)	P (10^{-8} eVcm)	Δ (eV)	γ_1	γ_2	γ_3	κ	F	m_{hh} (m_0)	E_{g1} (meV)
10	R FIR	RT	0.2	8								
11	SdH	1.2 – 4.2	0.24	7.1								
12	SdH	4.2	−0.19	6.6	0.38							
13	Theo		(−0.24)	6.7	0.48							0.4
14	R F/MIR	350	0.2	6.6								
15	T/R MIR	100 – 330	Ref. 14	Ref. 14	0.40							
16,17	SdH	4.2	−0.22	7.2	0.45	3	−0.5	0.17		0		
18	Far	100 – 293	$-0.206 + 2.6\times10^{-4}T/\mathrm{K}$	6								
19	Hall	4.2 – 300	-0.22 (Ref. 17) $+ 2.9\times10^{-4}T/\mathrm{K} + 7.9\times10^{-7}T^2/\mathrm{K}^2$	7.2 (Ref. 17) $+ 1.5\times10^{-3}T/\mathrm{K} + 7.8\times10^{-7}T^2/\mathrm{K}^2$	Ref. 17	Ref. 17	Ref. 17	Ref. 17		Ref. 17	−0.783	5.04
21	Theo		−0.1895	5.602	0.514	0.033	−0.356	−0.139		−2.54		
22	ThM	100 – 300	$-0.25 + 5\times10^{-4}T/\mathrm{K}$	$7.4 + 2\times10^{-3}T/\mathrm{K}$	Ref. 16	Ref. 16	Ref. 16	Ref. 16		Ref. 16		
23	SdH	77	−0.20	7.3	Ref. 16	Ref. 16	Ref. 16	Ref. 16	(−1.5)	Ref. 16		
24	MA MIR	4.2	−0.274	7.20	0.390	0.945	−0.03		−4.03	$-0.5 \le F \le 0$		
25,28	T MIR	10 – 295	$-0.26 + 8.3\times10^{-4}T/\mathrm{K}$	Refs. 16 and 17	0.40	2	−0.25	0.42	−0.58	−1		
27	T F/MIR	10 – 295	Ref. 25	$7.4 + 1.3\times10^{-3}T/\mathrm{K}$							−0.59 Ref. 25	
30	MA MIR	10 – 80	$-0.2733 + 1.02\times10^{-3}\frac{T^2/\mathrm{K}}{T+16\mathrm{K}}$	7.1	0.387	0.1	−0.5		−1.0	1.5		
31	SdH	4.2	Ref. 24	Ref. 24	Ref. 24	5.77	−1.17	−0.57	0.98	0 Ref. 24		
32,33	MA FIR	4.2	Ref. 30	7.0	Ref. 30	Ref. 30	0.2		−0.7			
34–36	MA MIR	4.2	−0.272	7.02	0.383	0.1	−0.5		−2.7	−0.5		

TABLE II. Optical constants for HgSe. The experimental method is given in Table I.

Ref.	T (K)	ϵ_∞	Γ (meV)	$\hbar/\tau$ (meV)
10	RT	12[a]		
43	RT	($n = 2.4, \lambda > 5$ μm)		
14	350	9[a]		
19	4.2 – 300	8.25		
20	95 – 300	12[a]		
25,28	10 – 295	$[n(0) = 4.3 - 2.7 \times 10^{-3} T/\mathrm{K}]$		
26	2 – 300	11	6	0.4 – 2.9
27	10 – 295	5.8 – 7.2		
29	2 – 300	6.5 – 7.5		0.7 – 3.7
37,38	10	Ref. 27		2

[a]The interband contribution was not considered in the determination of these values.

10^{18} cm^{-3} at 4.2 K as derived from van der Pauw measurements, assuming $n = 1/eR_H$ (where R_H is the Hall coefficient). The results are shown in Fig. 2. The relatively large scatter of the experimental points is probably due to the inaccuracy of the corresponding layer thicknesses because of the roughness of the as-grown epitaxial HgSe surface (see Ref. 3 for details). The resulting refractive index clearly shows an abrupt increase near 0.1 eV due to a decrease in the intraband absorption as well as a following decrease due to interband transitions. Theoretical curves of the refractive index for three different values of ϵ_∞ are also plotted in Fig. 2. Since the absolute values for the calculated refractive index depend significantly on the set of band structure parameters employed [see Sec. III A], the uncertainty in the derived values for ϵ_∞ is considerable. Based on all sets of band structure parameters listed in Table I, we estimate that $\epsilon_\infty = 7.5 \pm 1$. This value is compatible, within the estimated error, with the literature values of 8.25,[19] 6.6 ± 0.5,[27] and 7.3 ± 0.3,[29] but is considerably smaller than 11 ± 1 according to Ref. 26. Other values as reported in Refs. 10, 14, and 20 (see Table II) are not comparable because the interband contribution was not taken into account explicitly.

The absorption coefficient of several epitaxial HgSe layers was determined at several temperatures as described in Appendix B. Thereby we used the refractive index derived at 300 K independent of the actual temperature. Data reported in Refs. 25 and 27 and an extrapolation of the values for $Hg_{1-x}Cd_xSe$ in Ref. 39 to HgSe show a rather strong temperature dependence of the refractive index. However, the use of the different values for the refractive index results in absorption coefficients which are merely shifted by a nearly constant offset. In particular, the shift of the absorption edges

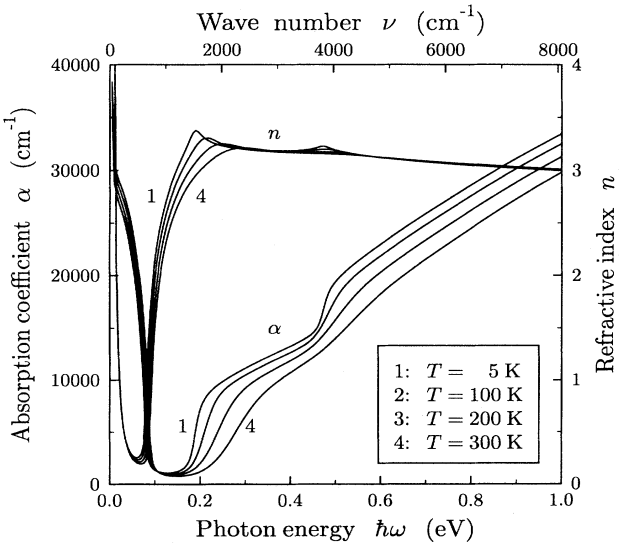

FIG. 1. Theoretical absorption coefficient and refractive index for HgSe with $N_D - N_A = 3 \times 10^{18}$ cm^{-3}. Band structure parameters have been taken from Ref. 19 together with $\epsilon_\infty = 8.0$, $\hbar/\tau = 3$ meV, and $\Gamma = 10$ meV.

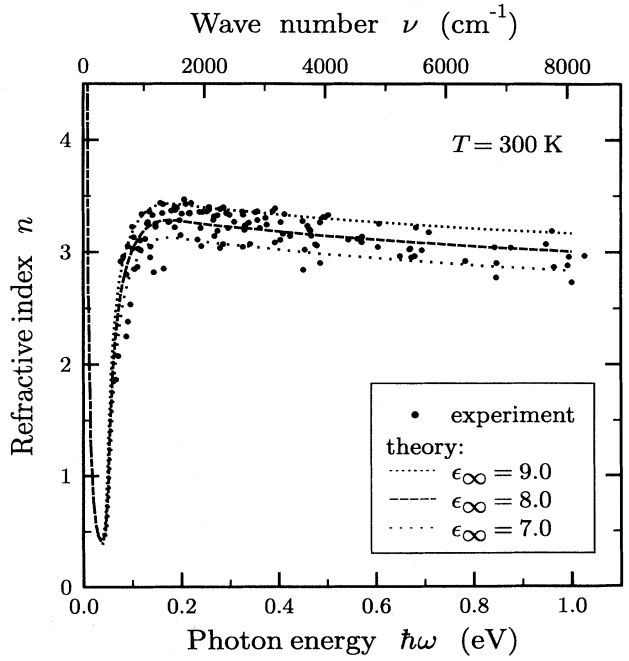

FIG. 2. Refractive index for HgSe at 300 K. Band structure parameters according to Ref. 19 together with $\hbar/\tau = 3$ meV and $\Gamma = 10$ meV have been employed for the theoretical curves.

discussed later in this section is not affected by this approximation. Figure 3 shows the results for a sample with a relatively high carrier concentration of 3.7×10^{18} cm^{-3} as determined from van der Pauw measurements at 4.2 K. Both the $\Gamma_8^{VB} \rightarrow \Gamma_8^{CB}$ and $\Gamma_6^{VB} \rightarrow \Gamma_8^{CB}$ interband transitions can clearly be seen as absorption edges at lower temperatures. We define the positions of the absorption edges by

$$\left.\frac{d^2\alpha(\omega)}{d\omega^2}\right|_{\omega_{edge}} = 0 \,. \tag{8}$$

It should be mentioned that $\hbar\omega_{edge}$ according to Eq. (8) is not equivalent to the transition energy at the Fermi wave vector $\boldsymbol{k}(E_F)$ but depending on temperature is shifted by a few meV to higher energies. The shift of the absorption edges with temperature as determined with Eq. (8) for the sample shown in Fig. 3 is displayed in Fig. 4. Both absorption edges shift linearly with temperature and the corresponding temperature coefficients are included in the figure. The resulting shift of the $\Gamma_8^{VB} \rightarrow \Gamma_8^{CB}$ transition nearly coincides with the data given in Ref. 15 for a sample with a carrier concentration of 4×10^{18} cm^{-3} (300 K) which is similar to that of our sample whose results are shown in Figs. 3 and 4. It should be mentioned that the temperature dependence of 1×10^{-4} eV/K according to Ref. 15 was determined by means of a different definition of the absorption edge than Eq. (8).

The shift of the absorption edge is primarily due to the temperature dependence of the E_0 gap which is not very well known for HgSe. Therefore we have used the results shown in Fig. 4 in order to determine dE_0/dT. Since HgSe is a semimetal and not a semiconductor, the fact that $dE_0/dT \neq d(\hbar\omega_{edge})/dT$ has to be considered. For this reason we have calculated the absorption coefficient using dE_0/dT as a variable until the temperature dependence of the $\Gamma_8^{VB} \rightarrow \Gamma_8^{CB}$ absorption edge $[d(\hbar\omega_{edge})/dT]$ coincided with the experimental value. We applied this fit procedure on the $\Gamma_8^{VB} \rightarrow \Gamma_8^{CB}$ and not the $\Gamma_6^{VB} \rightarrow \Gamma_8^{CB}$ absorption edge because of its larger temperature shift and the ability to more accurately determine the position of this edge. The net free donor concentration $N_D - N_A$ is used as an adjustable parameter to fit the theoretical to the experimental $\Gamma_8^{VB} \rightarrow \Gamma_8^{CB}$ absorption edge at $T = 4.2$ K. In order to reduce the number of fit parameters, we assumed a linear dependence for $E_0(T)$ instead of a nonlinear one as predicted, for instance, by Varshni.[40] This can be justified by our calculations which demonstrate, for the temperature range shown in Fig. 4, that a linear shift in the E_0 gap with temperature also results in a nearly linear shift of the $\Gamma_8^{VB} \rightarrow \Gamma_8^{CB}$ absorption edge which is consistent with our measurements. It should be mentioned that the shift of the $\Gamma_6^{VB} \rightarrow \Gamma_8^{CB}$ absorption edge can contain a considerable nonlinear component depending on the band structure parameters employed.

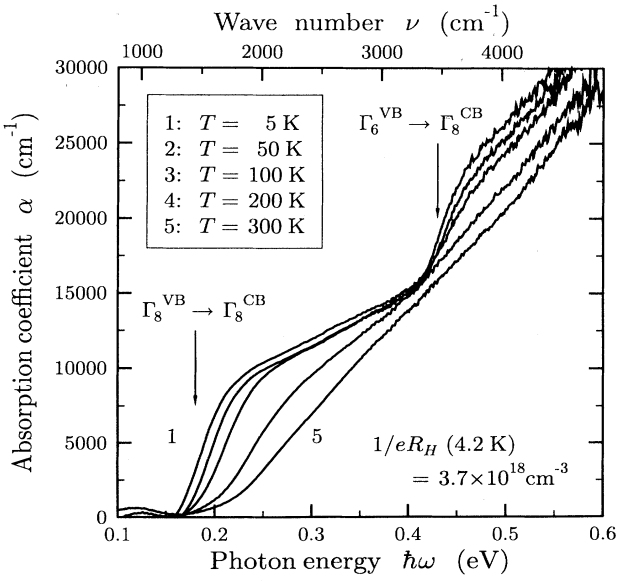

FIG. 3. Absorption coefficient of a HgSe sample at several temperatures. The van der Pauw measurement for this sample results in $1/eR_H$ (4.2 K) $= 3.7 \times 10^{18}$ cm^{-3}.

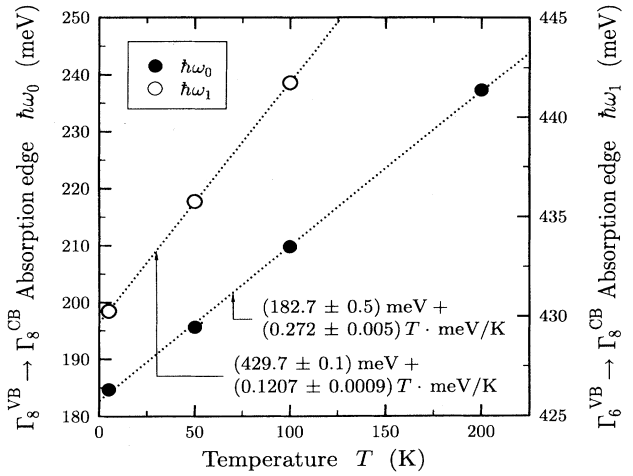

FIG. 4. Positions of the absorption edges versus temperature for the sample displayed in Fig. 3. The dotted curves are merely a least squares fit to the experimental data.

In Table III our results for dE_0/dT are summarized for the most important of the different sets of band structure parameters listed in Table I. For most band parameter sets we obtained $dE_0/dT = 0.70 - 0.77$ meV/K, however, the net free donor concentration had to be varied between 2.1 and 3.1×10^{18} cm^{-3}. The extremely low value determined with the band structure parameters from Ref. 19 is caused by the additional temperature dependence of the band parameter P assumed therein. The fourth and fifth columns of Table III list the differences and ratios between theory and experiment for the $\Gamma_6^{VB} \rightarrow \Gamma_8^{CB}$ absorption edge which was not included in the fit procedure. At $T = 0$ K the calculated absorption edge is displaced by up to 37 meV to higher energies and its temperature dependence can differ by up to a factor of 9 from the experimental value. Only the band structure parameters of Ref. 19 describe a reasonable fit of the temperature dependence of the $\Gamma_6^{VB} \rightarrow \Gamma_8^{CB}$ transition. On the other hand, the low value of approximately 0.5 meV/K for dE_0/dT as determined using these band

TABLE III. Temperature dependence of the E_0 gap (dE_0/dT) as determined from the temperature dependence of the $\Gamma_8^{VB} \rightarrow \Gamma_8^{CB}$ absorption edge in Fig. 4 for the different sets of band structure parameters. $N_D - N_A$ gives the net free donor concentration used in fitting the absorption edge at 4.2 K. The last two columns compare the results of the fit with the experimental position of the $\Gamma_6^{VB} \rightarrow \Gamma_8^{CB}$ absorption edge (difference between theory and experiment) and its temperature dependence (ratio of experiment to theory). It should be emphasized that the $\Gamma_6^{VB} \rightarrow \Gamma_8^{CB}$ absorption edge was not included in the fit procedure.

Source of band parameter (Ref.)	dE_0/dT (meV/K)	$N_D - N_A$ (10^{18} cm^{-3})	$\Gamma_6^{VB} \rightarrow \Gamma_8^{CB}$ $\hbar\omega_{edge}(0\,K)$ theor.−expt. (meV)	$\Gamma_6^{VB} \rightarrow \Gamma_8^{CB}$ $d(\hbar\omega_{edge})/dT$ expt./theor.
16,17	0.671	2.31	15	7.6
19	0.493	2.85	37	1.03
24	0.719	3.05	14	1.55
25,28	0.704	2.91	14	1.73
30	0.748	2.68	9	2.5
31	0.765	2.15	3	9.2
34–36	0.759	2.87	11	2.1

parameters is not consistent with the extrapolation from $Hg_{1-x}Cd_xSe$ to HgSe.[41,39] A definite conclusion about the validity of our results for dE_0/dT (0.70−0.77 meV/K) is difficult because of the large scatter in the values for dE_0/dT reported in the literature [0.26 meV/K,[18] 0.5 meV/K,[22] approximately 0.6 meV/K,[19] 0.72 meV/K,[41] 0.737 meV/K,[39] 0.83 meV/K,[25,28] and approximately 1.02 meV/K (Ref. 30)]. But it should be noted that the perhaps more reliable values reported in Refs. 41 and 39 from direct measurements of the E_0 gap of $Hg_{1-x}Cd_xSe$ fit our results very well.

By analyzing the shape of the experimental absorption edges it is possible to determine the broadening parameter Γ. It can be easily shown that the distance between the zero points of $d^3\alpha(\omega)/d\omega^3$ near the absorption edges at very low temperatures ($kT < \Gamma$) is approximately 2Γ. For most of our investigated samples we find that $\Gamma = 3 - 5$ meV for the $\Gamma_6^{VB} \rightarrow \Gamma_8^{CB}$ transition. Only a few samples have Γ values as large as 9 meV. No correlation between Γ and other parameters describing the structural quality of the layers such as x-ray rocking curve width could be observed. However, HgSe grown on nearly lattice matched ZnTe substrates usually has smaller values for Γ compared to that grown on highly lattice mismatched CdTe substrates.

At a given temperature the positions of the absorption edges are determined by the Fermi energy, i.e., the carrier concentration. An increase in the carrier concentration causes the Fermi energy and consequently the absorption edge to shift to higher energies (Burstein-Moss shift). Therefore a measurement of an absorption edge is a sensitive and direct method to determine the carrier concentration. Figure 5 shows the position of the $\Gamma_6^{VB} \rightarrow \Gamma_8^{CB}$ absorption edge for several samples with different Hall concentrations according to the van der Pauw method. The experimental values do not follow any of the theoretical curves. In contrast they are independent of the corresponding Hall concentration. Because the Fermi energy is directly determined by the positions of the absorption edges we assume that the optical measurements are correct and conclude that the van der Pauw measurements do not yield the correct carrier concentrations according to $n = 1/eR_H$. The usual interpretation of the van der Pauw results might be incorrect due to inhomogeneities in the HgSe layers.[42] This supposition is confirmed by the fact that the magnetoresistivity of some samples shows a linear instead of the expected quadratic dependence on the magnetic field. Furthermore, because the samples included in Fig. 5 were grown under different conditions, we conclude that the carrier concentration does not depend significantly on MBE growth parameters. In particular the observed dependence of the carrier concentration on the Hg/Se flux ratio as reported in Ref.

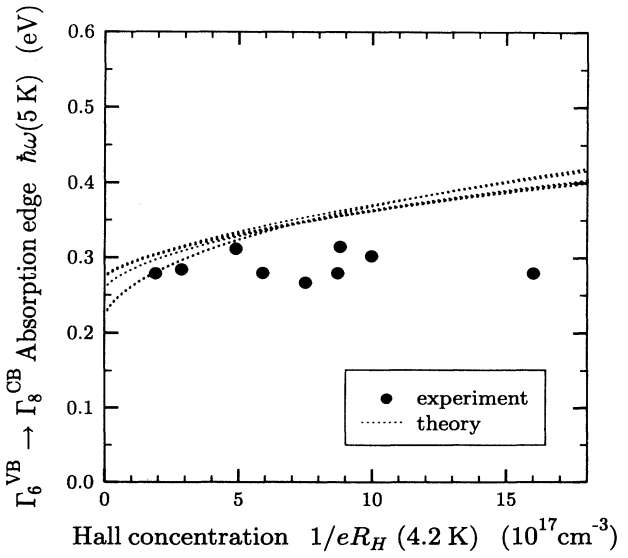

FIG. 5. Position of the $\Gamma_6^{VB} \rightarrow \Gamma_8^{CB}$ absorption edge at 5 K versus Hall carrier concentration at 4.2 K. The dotted lines are calculated using the band structure parameters of Refs. 16, 19, 24, 25, 28, 30, 31, and 34–36 by assuming that $n = 1/eR_H$.

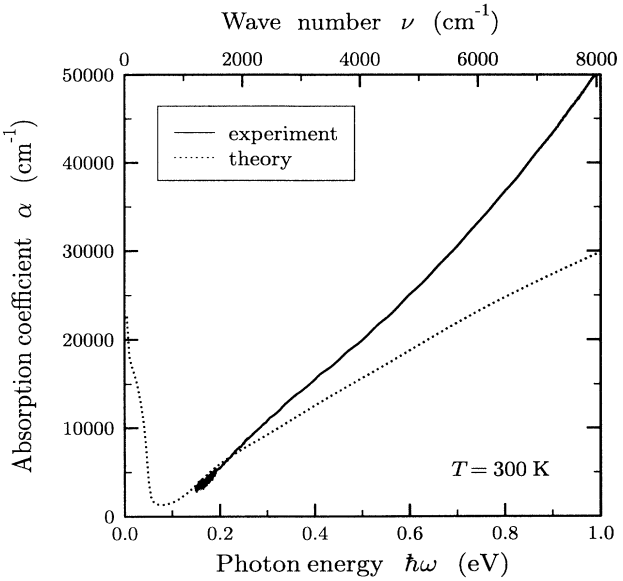

FIG. 6. Absorption spectra at 300 K. A typical experimental curve is compared with a theoretical calculation based on the band structure parameters of Ref. 19 for $N_D = 6 \times 10^{17}$ cm^{-3} and $\epsilon_\infty = 8.0$.

1 is based on van der Pauw measurements and does not coincide with our results based on optical absorption experiments.

In Fig. 6 a typical absorption spectrum at room temperature is plotted together with a theoretically calculated spectrum in order to compare the corresponding absolute values. All our measurements yield absorption coefficients which are larger than theoretically expected according to our calculations. This discrepancy between theory and experiment increases at larger photon energies. It is not possible to eliminate the discrepancy with any of the sets of band structure parameters as listed in Table I. Even the parameter set with the highest resulting absorption coefficient results in a ratio between experiment and theory of at least a factor of 1.5 at 1 eV. Furthermore, according to the HgSe literature, the experimental values for the absorption coefficient differ extremely from one investigation to the next. Compared to our experimental spectra the values of Refs. 43 and 44 are similar even though the samples of Ref. 43 are more highly doped, the values of Refs. 25 and 28 are smaller (nearly compatible to our theoretical calculations), whereas the spectra of Refs. 15 and 45 give much higher absorption coefficients. Other investigations have been carried out at lower photon energies and cannot be compared to our experiments.[46–48] At present we do not have an explanation for the inconsistency in the absorption data in the literature.

IV. E_1 AND $E_1 + \Delta_1$ GAPS

A. Theory

In the energy range from 2 to 4 eV the dielectric function for HgSe is dominated by transitions along the $\langle 111 \rangle$ directions (Λ) of the Brillouin zone. A doublet structure due to spin-orbit splitting corresponds to the E_1 ($\Lambda_{4,5}^{VB} \rightarrow \Lambda_6^{CB}$) and $E_1 + \Delta_1$ ($\Lambda_6^{VB} \rightarrow \Lambda_6^{CB}$) critical points (CP). The values for E_1 and $E_1 + \Delta_1$ for HgSe as reported in the literature are summarized in Table IV. Usually the E_1 and $E_1 + \Delta_1$ critical points are assumed to be nearly of type 2D M_1, i.e., the energy difference between the two corresponding bands is a two dimensional saddle point in $\boldsymbol{k}$ space.[49] The contribution of these 2D critical points to the dielectric function can be described by the following line shape function:[50]

TABLE IV. Literature values for E_1 and $E_1 + \Delta_1$ gaps of HgSe. The experimental method is given in the second column.

Ref.	Expt.	T (K)	E_1 (eV)	$E_1+\Delta_1$ (eV)
51	reflection	297	2.82[a]	3.13[a]
52	absorption	295	2.87[b]	3.20[b]
53	reflection	12	$\Delta_1 = 0.30$ eV	
44	transmission/refl.	RT	2.8	
54	reflection	290	2.8	
55	electroreflectance	RT	2.85	3.15
56	reflection	295	2.89	3.21
		20	3.03	3.34
57	reflection	RT	2.88	3.21
58,63	reflection	295	2.85	3.17
59	ellipsometry	RT	2.90	3.15
60	electroreflectance	RT	2.85	3.17
		77	2.946	3.223
61,63	ellipsometry	RT	2.781	3.120
62,63	ellipsometry	RT	2.797	3.159
1	reflection	RT	2.863	3.06

[a] $dE_1/dT = d(E_1 + \Delta_1)/dT = -0.43$ meV/K.
[b] $dE_1/dT = -0.46$ meV/K, $d(E_1 + \Delta_1)/dT = -0.38$ meV/K.

$$\epsilon(\omega) = \epsilon_{bg}(\omega) - \sum_{CP} A_{CP} e^{i\Phi_{CP}} \ln(\hbar\omega - E_{CP} + i\Gamma_{CP}) \ , \tag{9}$$

where the summation in Eq. (9) is carried out over the two critical points $E_{CP} = E_1$ and $E_{CP} = E_1 + \Delta_1$. By neglecting excitonic effects the phase angle Φ is equal to $\pi/2$ for a pure two dimensional saddle point. The background component ϵ_{bg} is a complex function and arises mainly from higher critical points (e.g., E_0',E_2).

B. Experimental results

Figure 7 shows a typical reflection spectra for HgSe in the E_1 and $E_1 + \Delta_1$ region at two different temperatures. Equations (9) and (7) together with the reflectivity R_{vs} (see Appendix A) were used to fit the reflection spectra. Since the line shape is not known for the higher transitions (i.e., for E_0',E_2,...) we assume a dispersion free ϵ_{bg} in Eq. (9). During the fit procedure we found that especially at higher temperatures the result is ambiguous as far as ϵ_{bg} and A_{CP} are concerned. Various combinations of these parameters yielded equally good fits. The reason for this is that at higher temperatures the shape of the reflection spectra does not contain sufficient structure to fit all of the parameters. But this disadvantage is not very important because the results for the most interesting parameters, E_1 and $E_1 + \Delta_1$, did not depend significantly on the rest of the parameters. The mean values at room temperature for eight HgSe samples are

$$E_1 = (2.80 \pm 0.02) \text{ eV},$$
$$E_1 + \Delta_1 = (3.05 \pm 0.03) \text{ eV},$$
$$\Gamma_{E_1} \approx \Gamma_{E_1+\Delta_1} = (0.11 \pm 0.01) \text{ eV} \ .$$

The above value for E_1 is in excellent agreement with ellipsometric measurements.[61–63] It is worth mentioning that most of the published values listed in Table IV were determined from reflection measurements by merely assuming that the position of the reflection maximum coincides exactly with the critical point energy. It can be easily shown that the reflection maximum is shifted away from the critical point energy by a few meV to higher energies because of the strong dispersion of the real component of the dielectric function (see Fig. 7). This explains why most of the values in Table IV with the exception of the ellipsometric data are higher than our values. Furthermore, our value for $E_1 + \Delta_1$ as well as the corresponding value reported in Ref. 1 for epitaxial HgSe is approximately 10 meV lower than all other values in Table IV for bulk HgSe. Also our value for Γ listed above is smaller than those reported in Refs. 61–63.

We have measured the reflectivity of HgSe as a function of temperature and determined the temperature dependence of the E_1 and $E_1 + \Delta_1$ gap as shown in Fig. 8. Within the accuracy of our measurements and fit procedure both gaps have quantitatively the same temperature dependence as judged by the near parallelism of the two sets of the experimental points in Fig. 8. Therefore we conclude that the spin-orbit splitting Δ_1 is independent of the temperature as is the case of other zinc blende materials (see, e.g., Ref. 64 for GaAs). The temperature dependence of E_1 and $E_1 + \Delta_1$ can be described either by the empirical relationship according to Varshni,[40]

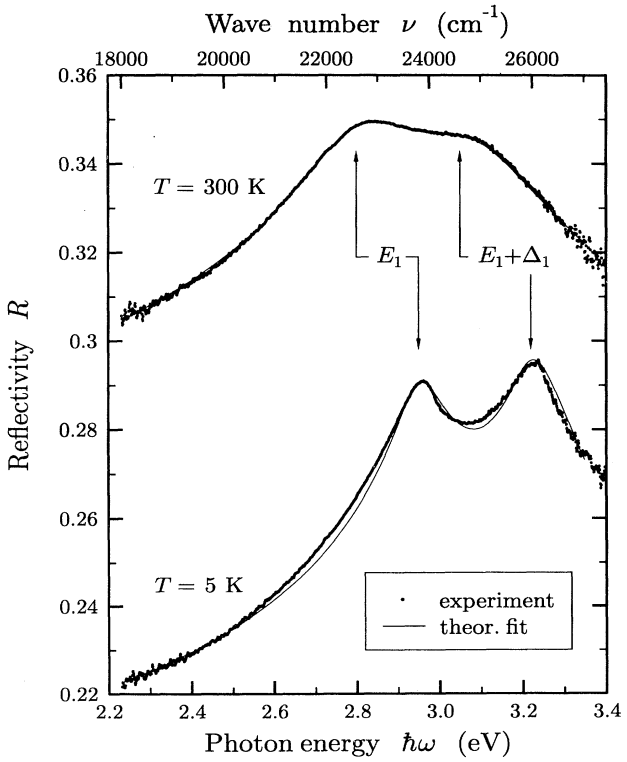

FIG. 7. Experimental and theoretically fitted reflectivity spectra of HgSe at 300 K and 5 K. The experimental and theoretical spectra for 300 K fall close together and consequently are nearly indistinguishable.

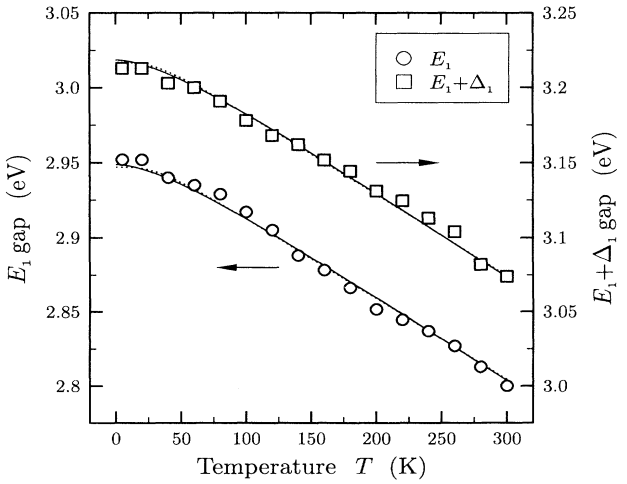

FIG. 8. E_1 and $E_1 + \Delta_1$ gaps of HgSe versus temperature. The lines are least squares fits to the experimental data using Eq. (10) (solid line) and Eq. (11) (dotted line). These two curves are nearly indistinguishable.

$$E(T) = E(0) - \frac{\alpha T^2}{T+\beta} , \quad (10)$$

or by an average Bose-Einstein statistical factor for phonon emission and absorption,[65]

$$E(T) = E_B - a_B \left[1 + \frac{2}{e^{\Theta/T} - 1}\right] . \quad (11)$$

A least squares fit of the values displayed in Fig. 8 based on Eq. (10) results in

$$E_1(0) = 2.949 \pm 0.002 \text{ eV} ,$$
$$\Delta_1 = 0.270 \pm 0.002 \text{ eV} ,$$
$$\alpha = 0.58 \pm 0.02 \text{ meV/K} ,$$
$$\beta = 60 \pm 12 \text{ K} ,$$

whereas the fit with Eq. (11) provides

$$E_B = 2.971 \pm 0.003 \text{ eV} ,$$
$$\Delta_1 = 0.270 \pm 0.002 \text{ eV} ,$$
$$a_B = 0.024 \pm 0.004 \text{ eV} ,$$
$$\Theta = 87 \pm 14 \text{ K} .$$

The above errors are the standard deviation of these parameters from the corresponding fit. Figure 8 displays the results of these two fitting procedures, which are almost indistinguishable. The derived temperature dependence coincides very well with the data from Refs. 51 and 56. Contrarily the corresponding values determined at 295 and 77 K in Ref. 60 suggest that the temperature dependences for the E_1 and $E_1 + \Delta_1$ gaps are different; their value for the temperature dependence of the $E_1 + \Delta_1$ gap is less than 50% of our value. However, we consider our results more reliable because our fit procedure is based on a larger number of data points.

Because of the above mentioned ambiguity in our fit procedure it is difficult to make quantitative statements about the temperature dependence of the line shape parameters (except the critical point energies) in Eq. (9). But by decreasing the temperature the resolution of the two maxima in the reflection spectra, which corresponds to the two critical points, increases distinctly as can be seen in Fig. 7. This is due to a decrease in the broadening parameters (Γ) with falling temperature. At 300 K the spectra can be described by $\Gamma_{E_1} \approx \Gamma_{E_1+\Delta_1} \approx 0.11$ eV, whereas at 5 K, $\Gamma_{E_1} \approx 0.05$ eV and $\Gamma_{E_1+\Delta_1} \approx 0.06$ eV were obtained.

V. CONCLUSION

The optical properties of epitaxially grown HgSe have been studied in detail over a wide range of frequencies covering the E_0, E_1, and $E_1 + \Delta_1$ gaps. In order to interpret the experimental transmission and reflection spectra, theoretical calculations of the dielectric function were carried out. This enabled us to derive fundamental material parameters for HgSe. The refractive index was determined at room temperature in the energy range up to 1 eV and thereby the background dielectric constant could be estimated. Absorption spectra from 5 to 300 K were derived in the energy region of the E_0 gap and yielded a linear temperature dependence for the observed absorption edges. Calculations based on several sets of band structure parameters yielded an estimation of the temperature dependence of the E_0 gap. Furthermore, we have observed and discussed differences in the carrier concentrations as determined from van der Pauw and optical measurements. Based on reflection measurements in the visible and ultraviolet region, critical point energies, E_1 and $E_1 + \Delta_1$, could be determined as a function of temperature and fitted to empirical relationships.

ACKNOWLEDGMENTS

The authors wish to thank V. Latussek for many helpful discussions. In addition we gratefully acknowledge the Deutsche Forschungsgemeinschaft and the Bundesministerium für Forschung und Technologie (Contract Number TK 0369) for financial support.

APPENDIX A: TRANSMISSION AND REFLECTION OF EPITAXIAL LAYERS

The transmission and reflection of a multilayer system is usually described with a matrix formalism, see, e.g., Ref. 66. For a single layer on a substrate it is also possible to reduce the matrix equation to explicit expressions for the transmission and reflection. In the following we use the subscripts v, l, and s to denote vacuum, layer, and substrate. The sequence of the subscripts for a transmission or reflection coefficient defines the incidence direction of the light: e.g., the reflection coefficient of the system (v,l,s,v) for the light falling on the layer is denoted by R_{vlsv} whereas R_{vslv} corresponds to the reflection coefficient of the same system but for light incident on the substrate. Furthermore we restrict our considerations to the case that the incident light is perpendicular to the interfaces. The deviation of $\leq 10°$ in our system was shown to have a negligible effect.

We do not describe the complete system (v,l,s,v) by a single matrix equation because this would lead to many narrowly spaced oscillations in the calculated transmission and reflection spectra corresponding to interference effects in the thick substrate. These interference fringes are usually not seen because a low spectral resolution is normally chosen. Therefore we use the matrix formalism to first calculate the transmission and reflection of the subsystem (v,l,s) corresponding to a substrate of infinite thickness. With these results we can describe the complete system (v,l,s,v) as a new system with only two interfaces; the simple (s,v) interface and an effective interface with reflection and transmission coefficients of the (v,l,s) system. By using intensities instead of electric fields in this calculation for the complete system, we automatically suppress any interference effects in the substrate. Thus for this complete two layer system

$$T_{vlsv} = T_{vslv} = \frac{T_{vls}T_{sv}A_s}{1 - R_{slv}R_{sv}A_s^2} ,$$

$$R_{vlsv} = R_{vls} + \frac{T_{vls}T_{slv}R_{sv}A_s^2}{1 - R_{slv}R_{sv}A_s^2} ,$$

$$R_{vslv} = R_{vs} + \frac{T_{vs}T_{sv}R_{slv}A_s^2}{1 - R_{slv}R_{sv}A_s^2} ,$$

where

$$T_{sv} = \frac{4}{n_s}\frac{n_s^2 + \kappa_s^2}{(n_s+1)^2 + \kappa_s^2} ,$$

$$T_{vs} = \frac{4n_s}{(n_s+1)^2 + \kappa_s^2} ,$$

$$R_{sv} = R_{vs} = \frac{(n_s-1)^2 + \kappa_s^2}{(n_s+1)^2 + \kappa_s^2} .$$

The following parameters which occur in these equations result from the matrix formalism for the (v,l,s) system:

$$T_{vls} = \frac{n_s^2}{n_s^2 + \kappa_s^2} T_{slv} ,$$

$$T_{slv} = \frac{1}{n_s}\frac{16(n_s^2+\kappa_s^2)(n_l^2+\kappa_l^2)A_l}{C_1 + C_2A_l + C_3A_l^2} ,$$

$$R_{vls} = \frac{C_4 + C_5A_l + C_6A_l^2}{C_1 + C_2A_l + C_3A_l^2} ,$$

$$R_{slv} = \frac{C_6 + C_7A_l + C_4A_l^2}{C_1 + C_2A_l + C_3A_l^2} ,$$

where

$$C_{\substack{1\\3}} = \left[(n_l \pm 1)^2 + \kappa_l^2\right]\left[(n_l \pm n_s)^2 + (\kappa_l \pm \kappa_s)^2\right] ,$$

$$C_{\substack{4\\6}} = \left[(n_l \mp 1)^2 + \kappa_l^2\right]\left[(n_l \pm n_s)^2 + (\kappa_l \pm \kappa_s)^2\right] ,$$

$$\begin{aligned} C_2 = {} & -2\cos\varphi_l[(n_l^2+\kappa_l^2-1)(n_l^2+\kappa_l^2-n_s^2-\kappa_s^2) \\ & -4\kappa_l^2 n_s + 4n_l\kappa_l\kappa_s] , \\ & +4\sin\varphi_l\{[\kappa_l(n_s+1) - n_l\kappa_s](n_l^2+\kappa_l^2-n_s) \\ & +\kappa_s(n_l - n_l n_s - \kappa_l\kappa_s)\} , \end{aligned}$$

$$\begin{aligned} C_{\substack{5\\7}} = {} & -2\cos\varphi_l[(n_l^2+\kappa_l^2-1)(n_l^2+\kappa_l^2-n_s^2-\kappa_s^2) \\ & +4\kappa_l^2 n_s - 4n_l\kappa_l\kappa_s] \\ & \mp 4\sin\varphi_l[\kappa_l(n_l^2+\kappa_l^2-n_s^2-\kappa_s^2) \\ & +(n_l^2+\kappa_l^2-1)(n_l\kappa_s - \kappa_l n_s)], \end{aligned}$$

$$\varphi_l = \frac{2\omega}{c} n_l d_l ,$$

$$A_l = \exp(-\alpha_l d_l) , \; A_s = \exp(-\alpha_s d_s) ,$$

$$\alpha_l = \frac{2\omega}{c}\kappa_l , \; \alpha_s = \frac{2\omega}{c}\kappa_s .$$

It is worthwhile mentioning that the above expression for T_{vlsv} coincides with the result given in the appendix of Ref. 67, however, we believe that the expression for T_{vls} according to Ref. 67 is not correct.

APPENDIX B: DETERMINATION OF OPTICAL CONSTANTS OF EPITAXIAL LAYERS

With the help of the equations derived in Appendix A it is in principle possible to determine the optical parameters $n_l(\omega)$ and $\alpha_l(\omega)$ of an epitaxial layer if the layer thickness d_l and the optical constants $[n_s(\omega)$ and $\alpha_s(\omega)]$ of the substrate are known. To accomplish this one has to measure the transmission $T_{vlsv}^{\text{meas}}(\omega)$ and the reflection $R_{vlsv}^{\text{meas}}(\omega)$ and subsequently determine the zero in the (n_l,α_l) plane of a function $f_1(n_l,\alpha_l)$ defined by

$$\begin{aligned} f_1(n_l,\alpha_l) = {} & [T_{vlsv}^{\text{meas}} - T_{vlsv}(n_l,\alpha_l)]^2 \\ & +[R_{vlsv}^{\text{meas}} - R_{vlsv}(n_l,\alpha_l)]^2 \end{aligned}$$

for each frequency ω. In practice, use of the above formula leads to refractive indexes with physically absurd oscillations. The most probable reason for this is that the absolute reflection cannot usually be measured with a sufficiently high accuracy. Therefore $n_l(\omega)$ and $\alpha_l(\omega)$ have to be determined separately whereby only the frequencies of the interference extrema in the reflectivity spectra are used. A first approximation for $n_l(\omega)$ at the position of the reflection extrema ω_{ex} is obtained by

$$n_l(\omega_{\text{ex}}) = \frac{m\pi c}{2d_l\omega_{\text{ex}}} ,$$

where m is the order of the interference extremum. This formula is strictly valid only for zero absorption and zero dispersion of both layer and substrate. With the resulting $n_l(\omega)$, $\alpha_l(\omega)$ can be determined from the zero of the function

$$f_2(\alpha_l) = [T_{vlsv}^{\text{meas}} - T_{vlsv}(n_l,\alpha_l)]^2 .$$

With the resulting $\alpha_l(\omega)$, $n_l(\omega_{\text{ex}})$ can be corrected in a first approximation by $\Delta n_l(\omega_{\text{ex}})$ according to

$$\left.\frac{dR_{vlsv}(n_l + \Delta n_l, \alpha_l)}{d\omega}\right|_{\omega_{\text{ex}}} = 0 .$$

The last two steps involving $f_2(\alpha_l)$ and $dR_{vlsv}/d\omega$ are repeated until the values for both $n_l(\omega)$ and $\alpha_l(\omega)$ converge. This was usually achieved after only two iterations.

[1] Y. Lansari, and J.W. Cook, Jr., and J.F. Schetzina, J. Electron. Mater. **22**, 809 (1993).

[2] C.R. Becker, L. He, S. Einfeldt, Y.S. Wu, G. Lérondel, H. Heinke, S. Oehling, R.N. Bicknell-Tassius, and G. Landwehr, J. Cryst. Growth **127**, 331 (1993).

[3] S. Einfeldt, H. Heinke, M. Behringer, C.R. Becker, E. Kurtz, D. Hommel, and G. Landwehr, J. Cryst. Growth **138**, 471 (1994).

[4] Y. Lansari, J. Ren, B. Sneed, K.A. Bowers, J.W. Cook, Jr., and J.F. Schetzina, Appl. Phys. Lett. **61**, 2554 (1992).

[5] J. Ren, D.B. Eason, L.E. Churchill, Z. Yu, C. Boney, J.W. Cook, Jr., J.F. Schetzina, and N.A. El-Masry, J. Cryst. Growth **138**, 455 (1994).

[6] G. Martinez, *Optical Properties of Semiconductors under Pressure*, Handbook on Semiconductors Vol. 2, edited by M. Balkanski (North-Holland, Amsterdam, 1980), Chap. 4C.

[7] W.G. Spitzer and H.Y. Fan, Phys. Rev. **106**, 882 (1957).

[8] E.O. Kane, J. Phys. Chem. Solids **1**, 249 (1957).

[9] E.O. Kane, in *Semiconductors and Semimetals*, edited by R.K. Willardson and A.C. Beer (Academic, New York, 1966), Vol. 1, p. 75.

[10] G.B. Wright, A.J. Strauss, and T.C. Harman, Phys. Rev. **125**, 1534 (1962).

[11] C.R. Whitsett, Phys. Rev. **138**, A829 (1965).

[12] L.M. Bliek and G. Landwehr, Phys. Status Solidi **33**, K67

(1969).
[13] H. Overhof, Phys. Status Solidi B **43**, 221 (1971)
[14] V.V. Volkov, L.V. Volkova, and P.S. Kireev, Fiz. Tekh. Poluprovodn. **4**, 1437 (1970) [Sov. Phys. Semicond. **4**, 1230 (1971)].
[15] V.V. Volkov, V.M. Bezborodova, V.P. Dmitriev, A.V. Vanyukov, and P.S. Kireev, Fiz. Tekh. Poluprovodn. **4**, 1443 (1970) [Sov. Phys. Semicond. **4**, 1234 (1971)].
[16] R.R. Galazka, W.M. Becker, and D.G. Seiler, J. Phys. Chem. Solids Suppl. **32**, 481 (1971).
[17] D.G. Seiler, R.R. Galazka, and W.M. Becker, Phys. Rev. B **3**, 4274 (1971).
[18] V.V. Volkov, L.V. Volkova, and P.S. Kireev, Fiz. Tekh. Poluprovodn. **7**, 605 (1973) [Sov. Phys. Semicond. **7**, 420 (1973)].
[19] S.L. Lehoczky, J.G. Broerman, D.A. Nelson, and C.R. Whitsett, Phys. Rev. B **9**, 1598 (1974).
[20] A. Manabe and A. Mitsuishi, Solid State Commun. **16**, 743 (1975).
[21] L.M. Bliek and H. Overhof, Phys. Status Solidi B **69**, 163 (1975).
[22] T. Dietl and A. Jedrzejczak, Phys. Status Solidi B **71**, K39 (1975).
[23] P. Byszewski, J. Kowalski, and R.R. Galazka, Phys. Status Solidi B **78**, 477 (1976).
[24] Y. Guldner, C. Rigaux, M. Dobrowolska, A. Mycielski, and W. Dobrowolski, in *Physics of Narrow Gap Semiconductors*, Proceedings of the 3rd International Conference on Physics of Narrow Gap Semiconductors, edited by J. Rauluszkiewicz, M. Gorska, and E. Kaczmarek (Elsevier, Amsterdam, 1978), p. 87.
[25] W. Szuszkiewicz, in *Physics of Narrow Gap Semiconductors* (Ref. 24), p. 93.
[26] A. Manabe, H. Noguchi, and A. Mitsuishi, Phys. Status Solidi B **90**, 157 (1978).
[27] W. Szuszkiewicz, A.M. Witowski, and M. Grynberg, Phys. Status Solidi B **87**, 637 (1978).
[28] W. Szuszkiewicz, Phys. Status Solidi B **91**, 361 (1979).
[29] A.M. Witowski and M. Grynberg, Phys. Status Solidi B **100**, 389 (1980)
[30] M. Dobrowolska, W. Dobrowolski, and A. Mycielski, Solid State Commun. **34**, 441 (1980).
[31] R.R. Galazka, W. Dobrowolski, and J.C. Thuillier, Phys. Status Solidi B **98**, 97 (1980).
[32] K. Pastor, M. Jaczynski, and J.K. Furdyna, J. Phys. Soc. Jpn. Suppl. **49**, A779 (1980).
[33] K. Pastor, M. Jaczynski, and J.K. Furdyna, Phys. Rev. B **24**, 7313 (1981).
[34] A. Mycielski, J. Kossut, M. Dobrowolska, and W. Dobrowolski, in *Physics of Semiconducting Compounds*, Proceedings of the 11th Conference on Physics of Semiconducting Compounds, edited by J. M. Langer (Ossolineum, Wroclaw, 1982), p. 122.
[35] A. Mycielski, J. Kossut, M. Dobrowolska, and W. Dobrowolski, in *Physics of Narrow Gap Semiconductors*, Proceedings of the 4th International Conference on Physics of Narrow Gap Semiconductors, edited by E. Gornik, H. Heinrich, and L. Palmetshofer, Lecture Notes in Physics Vol. 152 (Springer, Berlin, 1982), p. 211.
[36] A. Mycielski, J. Kossut, M. Dobrowolska, and W. Dobrowolski, J. Phys. C **15**, 3293 (1982).
[37] W. Szuszkiewicz and A.M. Witowski, in *Physics of Semiconducting Compounds*, Proceedings of the 12th Conference on Physics of Semiconducting Compounds (Ossolineum, Wroclaw, 1983), p. 195.
[38] W. Szuszkiewicz and A.M. Witowski, Solid State Commun. **48**, 821 (1983).
[39] C.J. Summers and J.G. Broerman, Phys. Rev. B **21**, 559 (1980).
[40] Y.P. Varshni, Physica **34**, 149 (1967).
[41] P.A. Slodowy and W. Giriat, Phys. Status Solidi B **48**, 463 (1971).
[42] A.C. Beer, *Galvanomagnetic Effects in Semiconductors*, (Academic, New York, 1963), Suppl. 4.
[43] H. Gobrecht, U. Gerhardt, B. Peinemann, and A. Tausend, J. Appl. Phys. Suppl. **32**, 2246 (1961).
[44] M.V. Kot and V.A. Mshenskii, Izv. Akad. Nauk SSSR Ser. Fiz. **28**, 1023 (1964) [Bull. Acad. Sci. USSR Phys. Ser. **28**, 924 (1964)].
[45] P.S. Kireev and V.V. Volkov, Fiz. Tekh. Poluprovodn. **7**, 1419 (1973) [Sov. Phys. Semicond. **7**, 949 (1974)].
[46] T.C. Harman and A.J. Strauss, J. Appl. Phys. Suppl. **32**, 2265 (1961).
[47] F.F. Kharakhorin, and V.M. Petrov, Fiz. Tekh. Poluprovodn. **1**, 143 (1967) [Sov. Phys. Semicond. **1**, 112 (1967)].
[48] L.G. Volzhenskaya, V.E. Krevs, and M.V. Pashkovskii, Fiz. Tekh. Poluprovdn. **6**, 774 (1972) [Sov. Phys. Semicond. **6**, 674 (1972)].
[49] M. Cardona, *Modulation Spectroscopy* (Academic, New York, 1969), Suppl. 11.
[50] D.E. Aspnes, *Modulation Spectroscopy/Electric Field Effects on the Dielectric Function of Semiconductors*, Handbook on Semiconductors Vol. 2, edited by M. Balkanski (North-Holland, Amsterdam, 1980), Chap. 4A.
[51] M. Cardona, J. Appl. Phys. **32S**, 2151 (1961).
[52] M. Cardona and G. Harbeke, J. Appl. Phys. **34**, 813 (1963).
[53] W.J. Scouler and G.B. Wright, Phys. Rev. **133**, A736 (1964).
[54] V.V. Sobolev, Opt. Spektrosk. **18**, 813 (1965) [Opt. and Spectrosc. (USSR) **18**, 456 (1965)].
[55] M. Cardona, K.L. Shaklee, and F.H. Pollak, Phys. Rev. **154**, 696 (1967).
[56] I.N. Borisov, V.V. Mikhailin, and P.S. Kireev, Izv. Akad. Nauk. Arm. SSR Fiz. **6**, 61 (1971).
[57] I.N. Borisov, V.V. Mikhailin, P.S. Kireev, and V.M. Bezborodova, Fiz. Tekh. Poluprovodn. **5**, 822 (1971) [Sov. Phys. Semicond. **5**, 728 (1971)].
[58] I.N. Borisov, P.S. Kireev, V.V. Mikhailin, and V.M. Bezborodova, Fiz. Tekh. Poluprovodn. **5**, 829 (1971) [Sov. Phys. Semicond. **5**, 734 (1971)].
[59] A. Moritani, H. Sekiya, K. Taniguchi, C. Hamaguchi, J. Nakai, and R. Makabe, Jpn. J. Appl. Phys. **10**, 1410 (1971).
[60] A. Moritani, C. Hamaguchi, and J. Nakai, J. Phys. Soc. Jpn. **32**, 1151 (1972).
[61] K. Kumazaki, L. Viña, C. Umbach, and M. Cardona, Solid State Commun. **68**, 591 (1988).
[62] K. Kumazaki, L. Viña, C. Umbach, and M. Cardona, Phys. Status Solidi B **156**, 371 (1989).
[63] K. Kumazaki, J. Cryst. Growth **101**, 687 (1990).
[64] P. Lautenschlager, M. Garriga, S. Logothetidis, and M. Cardona, Phys. Rev. B **35**, 9174 (1987).
[65] L. Viña, S. Logothetidis, and M. Cardona, Phys. Rev. B **30**, 1979 (1984).
[66] D. Fasold, K. Hehl, and S. Jetschke, Phys. Status Solidi A **86**, 125 (1984).
[67] R. Swanepoel, J. Phys. E **16**, 1214 (1983).